RECOMMENDATION ITU-R RS.1449*

FEASIBILITY OF SHARING BETWEEN THE FSS (SPACE-TO-EARTH) AND THE EARTH EXPLORATION-SATELLITE (PASSIVE) AND SPACE RESEARCH (PASSIVE) SERVICES IN THE BAND 18.6-18.8 GHz

(Question ITU-R 215/7)

(2000)

The ITU Radiocommunication Assembly,

considering

a) that the 18.6-18.8 GHz band is allocated to the FSS (space-to-Earth) on a primary basis;

b) that the 18.6-18.8 GHz band is allocated to the Earth exploration-satellite service (EESS) (passive) and space research service (SRS) (passive) on a primary basis in Region 2 and on a secondary basis in Regions 1 and 3;

c) that RR No. S5.523 states that administrations are requested to limit as far as practicable the pfd at the Earth's surface in the band 18.6-18.8 GHz, in order to reduce the risk of interference to passive sensors in the EESS and space research service;

d) that passive sensing in this band is necessary to obtain critical environmental measurements on a worldwide basis and no other frequency band is available that could replace this band;

e) that the band 18.6-18.8 GHz is very important for use by FSS in view of the large number of systems in the planning stage and of the presence of some systems already in operation;

f) that studies have been conducted assessing the aggregate interference into a passive spaceborne sensor from multiple FSS transmitting satellites, all utilizing spot beams and having a common service area, and have found that constraints are needed on both FSS and EESS (passive) systems if sharing is to take place (see Annex 1);

g) that studies have shown that FSS satellites in 8, 12 and 24 h highly elliptical orbits (HEO) cause less interference to the sensor than GSO FSS satellites (see Annex 2),

recommends

1 that passive sensors operating in the EESS and SRS and acquiring data over land masses be designed to collect data only when travelling north in the northern hemisphere and south in the southern hemisphere and utilize an antenna that is inclined about 40° from nadir and scans in azimuth about the velocity vector of the spacecraft;

2 that passive sensors be designed to operate in an interference environment based on a pfd produced by a FSS at the surface of the Earth limited to –95 dB(W/m^2) across the 18.6-18.8 GHz band; this value could be exceeded by up to 3 dB for no more than 5% of the time.

ANNEX 1

An evaluation of potential interference into the EESS (passive) in the 18.6-18.8 GHz band from GSO satellites operating in the FSS

1 Introduction

Spaceborne microwave science sensors make use of very narrow beam antennas to obtain such information as surface temperature, moisture content, sea state and others. Certain passive sensors make use of the 18.6-18.8 GHz band. This same band is shared with GSO satellite systems operating in the FSS. There is potential for excessive interference into the passive sensors from these GSO satellites. This would be dominated by energy scattered from terrestrial targets into

* Radiocommunication Study Group 7 made editorial amendments to this Recommendation.

the receiving antennas of these passive sensors. The level of interference is affected by: the individual GSO pfd; number of simultaneous GSO systems; methods of frequency reuse within the FSS; the reflectivity of the terrain as characterized by the terrain scattering coefficient; and the mode of operation of the spaceborne sensor. In the United States of America, passive sensors have a primary allocation in the 18.6-18.8 GHz band. The United States of America limits the FSS pfd to –101 dB(W/(m^2 · 200 MHz)). Internationally, passive sensors have a primary allocation in Region 2 and secondary allocations in Regions 1 and 3. RR Table S21.4 limits FSS pfd to –92 dB(W/(m^2 · 200 MHz)) at low elevation angles up to –82 dB(W/(m^2 · 200 MHz)) and higher elevation angles.

Consequently, there is a potential of pfd from the FSS from –101 dB(W/(m^2 · 200 MHz)) to –82 dB(W/(m^2 · 200 MHz)) globally. Since the spaceborne passive sensors would be exposed only intermittently to scattered energy from FSS coverage areas, it is of interest to determine the rate of occurrence of excessive interference events. Recommendation ITU-R RS.1029 states that in shared frequency bands (except in the absorption bands), the interference levels given above (–155 dB(W/100 MHz) for 18.6-18.8 GHz) can be exceeded for less than 5% of all measurement cells within a sensor's service area in the case where the loss occurs randomly, and for less than 1% of measurement cells in the case where the loss occurs systematically at the same locations.

The objective of this work is to identify the areas of excessive interference for the different levels of potential FSS pfd. The criteria from Recommendation ITU-R RS.1029 indicate the appropriate metric for interference depends on the particular sensor application and the nature of the interference that occurs. Herein, we report estimates for both conditional events (rate of occurrence given the spaceborne sensor is within a FSS coverage area) and unconditional events (rate of occurrence globally).

A secondary goal is to evaluate potential interference mitigation techniques and to describe a potential method of mitigating interference by avoiding geometry where the sensor might be pointed directly, or nearly so, into a specular reflection. It has been suggested that additional mitigation could be achieved by restricting the sensor scan range from ±70° to ±35°. Both methods were evaluated for a specific case of 4, 8, and 16 GSO systems in the FSS simultaneously serving a coverage area described with 24 spot beams.

The approach was to make use of Monte-Carlo simulations where the interference into a spaceborne sensor is estimated as it orbits the Earth. The motion of the GSO satellites, the Earth, and the spaceborne sensor are all accounted for. Since the scattering of energy from the Earth's surface is a random phenomenon (due to independent fading effects and terrain variability), this variability is also included in the simulation. At each simulation time instant, the interference from all 16 satellites was accounted for including the weighting by the directivity and angular offset of the individual spot beams.

2 Interference scenario

It is of interest to estimate a worst-case level of interference into an EESS satellite passive sensor from a maximum constellation of 16 FSS satellite systems that each provides a common coverage area that is described by 22 conterminous beams and two nearby, but geographically separate beams. Each of the systems uses four times frequency segmentation to minimize intra-system interference. The 16 satellite systems are then grouped by systems of four that offset their segmentation choices to further minimize inter-system interference. Further reduction of mutual interference is achieved by a 2° orbital separation between systems.

Figure 1 illustrates a microwave passive sensing satellite passing over a FSS coverage area and receiving interference from the ground reflections. The sensor makes use of a highly directive receiving beam that is scanned ±70° perpendicular to the direction of motion. The sensing area is very small compared to the FSS spot beams that make up the total FSS coverage area. In the simulations performed for this work, the interference is calculated at 2° increments of scan.

As mentioned, each system will segment its spectrum to minimized intra-system interference. Figure 2 illustrates the isolation of four spot beams by such segmentation. The pattern is repeated throughout the coverage area. The next three systems will, it is assumed, stagger the segmentation so the second system, for example, might use F2 in place of F1, F3 in place of F2, etc. Additional systems after the fourth will simply repeat the pattern. Isolation of the systems will be

aided by spatial separation in orbit at 2° increments and use of directive antennas by terrestrial-based users. By this scenario each of the 22 conterminous spot beams will scatter power from four GSOs with spectrum that overlaps that of the EESS, as well as other GSOs that contribute through side lobes that overlap from adjacent beams.

FIGURE 1

16 GSO FSS systems interfering with spaceborne sensor

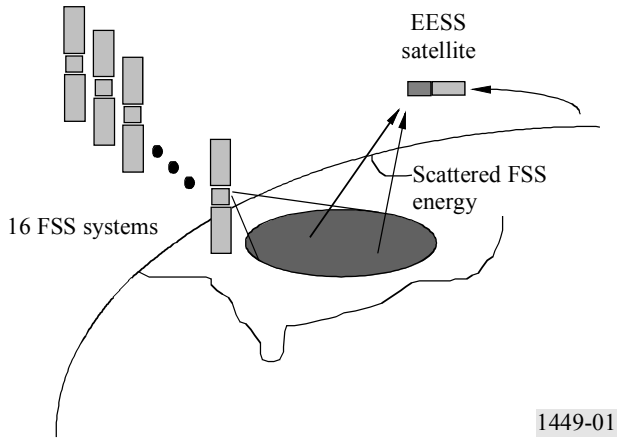

FIGURE 2

Typical FSS coverage, 22 conterminous beams and two off-shore beams

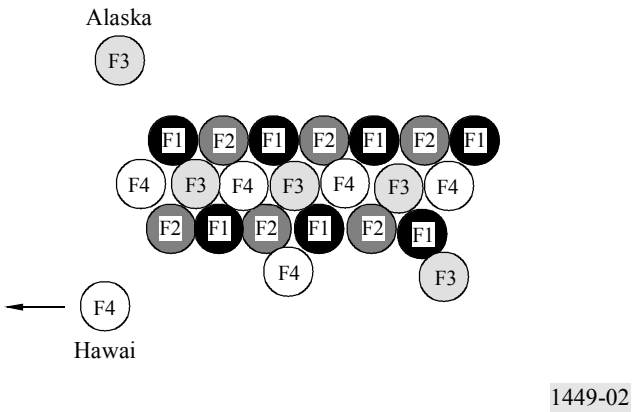

In the event such intra-service interference mitigation techniques are not used, it is possible that all satellites would use identical frequency segmentation. In that case each spot would scatter energy from 16 satellites. However, since the spots would still have the F1-F4 allocation pattern, only a subset of these spots would scatter energy that overlapped the EESS band. In the scenario shown in Fig. 2 this could range from 5 to 7 spot beams depending on the selections of F1-F4 segments.

A set of typical characteristics for the FSS and EESS systems are described in Tables 1 and 2 respectively. The scattering coefficient model described in § 3 is used as the basis for estimating the scattered power.

TABLE 1

FSS parameters in the 18.6-18.8 GHz band

Coverage	22 conterminous, 2 off-shore
5 dB beamwidth	1.0°
Maximum antenna gain	46.5 dBi
pfd at surface of the Earth	−101.0 dB(W/(m^2 · 200 MHz)) each polarization
Polarization	RHC and LHC each beam
Bandwidth	200 MHz
Frequency reuse	Every fourth beam
Antenna pattern	Recommendation ITU-R S.672 with $L_N = -25$ dB and $L_F = 0$ dBi

TABLE 2

Spaceborne passive sensor parameters in the 18.6-18.8 GHz band

Orbital altitude	500 km	
Orbital inclination	90.0°	
Boresight elevation angle	–45.0°	
Antenna pattern	dBi	Off-axis angle, θ
	57.0	θ ≤ 0.2°
	21.0	0.2° < θ ≤ 5.5°
	–14.0	5.5° < θ ≤ 90.0°
	–17.0	θ > 90.0
Antenna scan angle	±70°	
Polarization	Linear	
Receiver reference bandwidth	100.0 MHz	
Interference threshold	–155 dB(W/100 MHz)	
Along scan spatial resolution	2 km	
Across scan spatial resolution	2 km	
Circular to linear polarization loss	1.5 dB	
Basis for scattering estimates	Skylab/University of Kansas, backscatter curve fits and facet theory (see § 3)	

3 Scattering model

A critical parameter affecting the level of interference into a spaceborne sensor is the terrestrial reflectivity as indicated by the scattering coefficient of the terrain being viewed by the sensor. This can result in energy being scattered backwards toward its GSO FSS source and being intercepted by a spaceborne sensor that is moving away from the GSO nadir. Alternatively, the energy can be scattered forward and intercepted by a sensor that is moving toward the GSO nadir. There is much more data on backscatter phenomena than for the forward scatter case. Herein we attempt to make use of available backscatter data and extrapolations, and to infer from these the forward scatter effects.

3.1 Backscatter coefficients

Several methods have been proposed in open literature for modelling the mean and extreme values for backscattering coefficients. Scatterometer data from Skylab, as shown in Fig. 3, indicate a dependence on incidence angle that varies rapidly over the range of 0-10°. The maximum is at 0° incidence.

FIGURE 3

Data from Skylab S-193 scatterometer

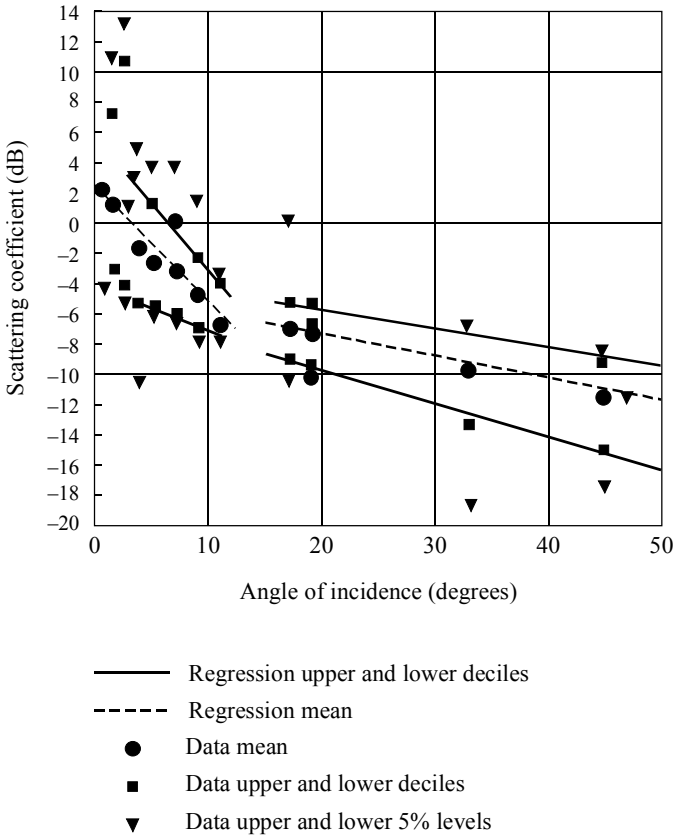

Regression lines shown for mean $0° < \theta < 11°$, $17° < \theta < 45°$.
Deciles $3.5° < \theta < 11°$, $17° < \theta < 45°$.

1449-03

Beyond 10° incidence, the scattering coefficient continues to decrease but at a significantly slower rate. The region from 0-10° is regarded as a surface specular response, whereas the region beyond is regarded as a surface diffuse response. Since the Skylab data is a composite of many surface types, the different regions cannot be associated with any particular type. Curve fits are shown for the mean as well as the 10th and 90th percentiles. Note that the upper and lower

percentiles are not symmetric with the mean. Also note the width of the percentile range is a maximum at normal incidence and diminishes to a minimum at about 10° incidence. At that point it gradually increases out to 50° incidence. At normal incidence the mean is slightly more than 2 dB. The fit to the upper percentile would suggest a value of about 6 dB at normal incidence.

Several models have also been proposed for statistical distributions of the backscatter coefficients. When a sensor beam is filled with homogeneous terrain, an appropriate model for the received signal using a square law detector is an exponential probability density. For complex terrain, the log-normal probability density and variations have been proposed. Since the Skylab data represents a composite of many types of terrain (the entire United States of America territory), the log-normal density is made use of herein to approximate the statistical distribution of the scattering coefficient. The mean of the scattering coefficient is extrapolated from the Skylab and other available data. The log-normal parameters are inferred by assuming a log-normal process that produces the extrapolated mean and replicates the Skylab observed variability. The resulting mean and percentiles of the scattering coefficient are shown in Fig. 4. As noted before, the percentiles are not symmetrically disposed about the mean. Also, the absolute levels do not differ greatly from the Skylab measurements at 13.9 GHz.

FIGURE 4

Scattering coefficient model for 18.6-18.8 GHz
(Mean and percentiles)

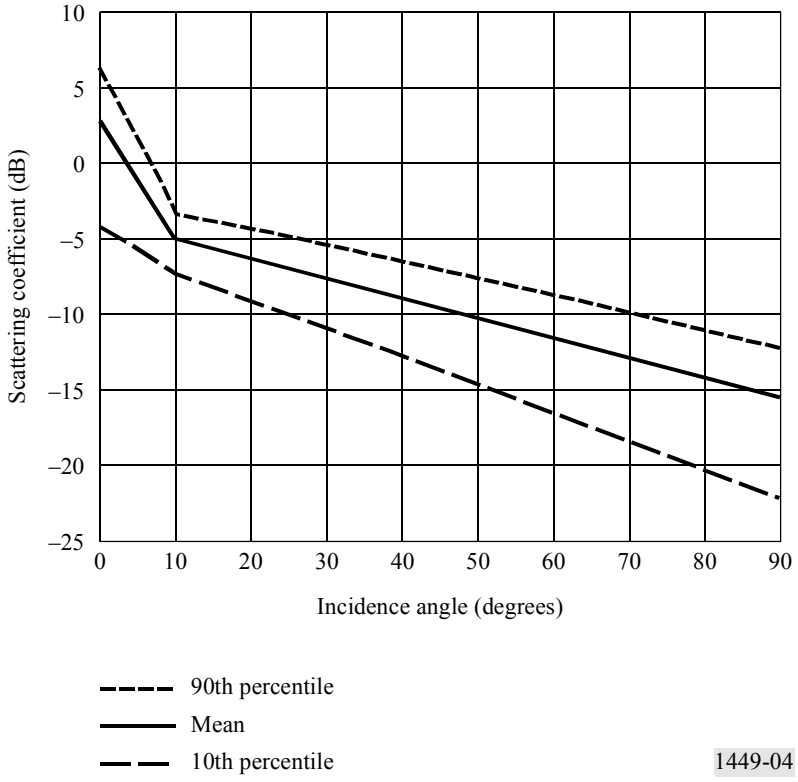

Figure 5 illustrates the log-normal parameters necessary to fit the extrapolated mean and variability at 18.6-18.8 GHz. The derived median is close to the mean but it is not the same, nor need it be. The standard deviation is near 4 dB at 0° incidence, a minimum at about 10° incidence and gradually increases to about 4 dB at 90° incidence.

Using these parameters, the scattering coefficient would have the approximate cumulative distributions as shown in Fig. 6. While at normal incidence, the upper percentile is near 6 dB. The upper percentile at 10° incidence is considerably less, near –4 dB. Since the spaceborne passive sensor will be designed to view the Earth at oblique angles near 40°, one can see from the trends in Figs. 5 and 6 that the upper percentile could be considerably less than what one would expect at normal incidence.

FIGURE 5

Log-normal parameters of distribution at 18.6-18.8 GHz

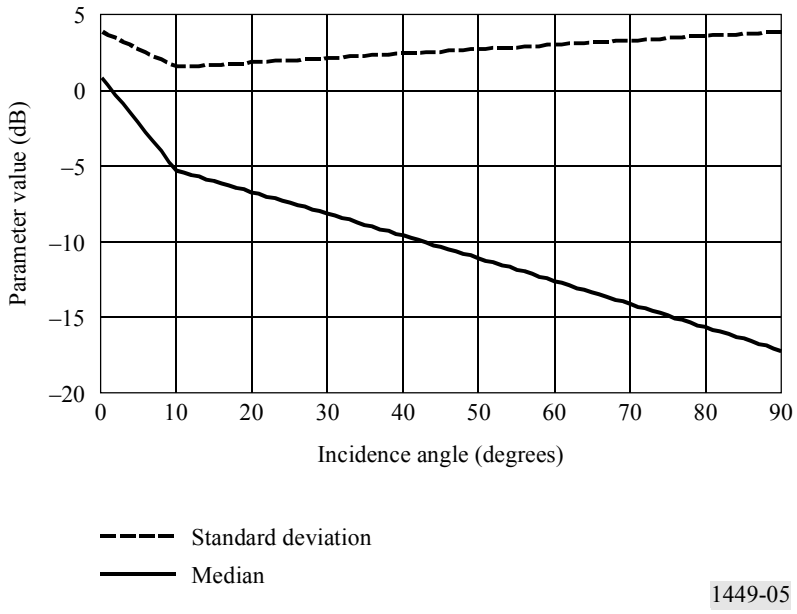

FIGURE 6

Cumulative distribution of scattering coefficient at normal and 10° incidence

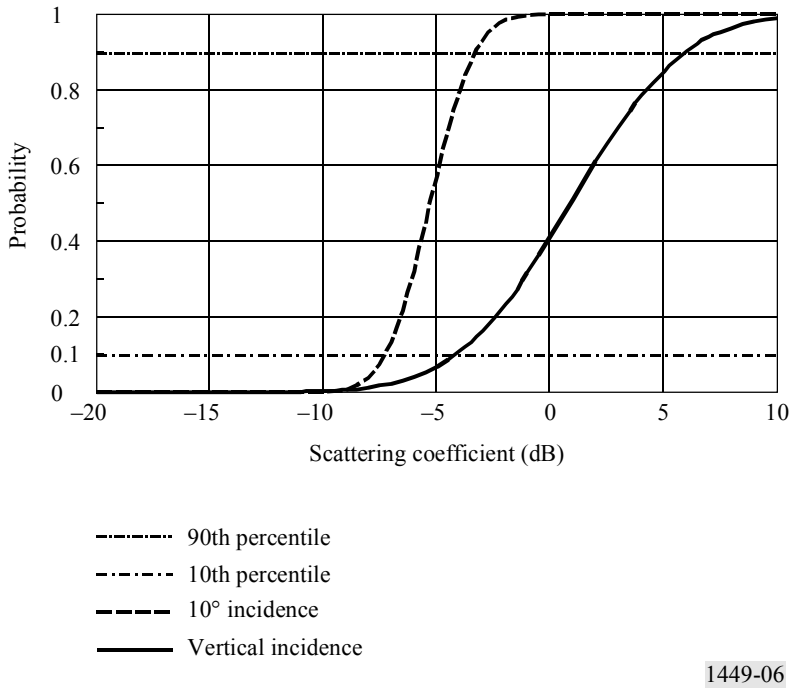

3.2 Bistatic scattering coefficients

It has been suggested that one could create a bistatic scattering coefficient model from backscatter data by assuming the surface of the Earth could be approximated by an array of flat facets. This makes use of a geometric optics approximation where the reflected rays are treated as line segments.

Figure 7 shows an incident ray impinging on a facet oriented at an angle Φ_x with respect to the vertical. The normal to this facet bisects the included angle between the incident and scattered ray. The percentage of facets with such an orientation would be indicated by the previous backscatter relation at the angle Φ_x. Hence, for a (Φ_i, Φ_s) pair, we get the corresponding scattering coefficient by extracting that value from the data fit at an intermediate angle corresponding to Φ_x. From the geometric relation above:

$$\Phi_x = (\Phi_i - \Phi_s)/2$$

If we redefine Φ_s as:

$$\Phi_s = \Phi_i + \Delta\Phi_s$$

then Φ_s is viewed as being referenced to the specular direction, which is identical to the incidence angle, Φ_i.

Substituting the modification, then:

$$\Phi_x = -\Delta\Phi_s/2$$

that is, Φ_x has a magnitude of one-half the amount by which Φ_s differs from the specular angle. Also, the direction of Φ_x is opposite to that of $\Delta\Phi_s$, being negative if Φ_s exceeds Φ_i, and positive if Φ_s is less than Φ_i.

Thus we can estimate the forward scattering coefficient, as referenced to the specular direction, as:

$$\sigma_s(\Delta\Phi_s) = \sigma_0(-\Delta\Phi_s/2)$$

where σ_s is the desired scattering coefficient and σ_0 is the reference backscatter coefficient (σ_s and σ_0 are conventional symbols for the scattering coefficient and should not be confused with the standard deviation used in previous sections). Note that for $\Phi_s = \Phi_i$, Φ_x is always zero and the corresponding σ_0 is that which occurs at the peak of the backscatter relation, that is, always corresponding to the number of facets at zero elevation. Also, when $\Phi_s = -\Phi_i$ ($\Delta\Phi_s = -2\Phi_i$ and the scattered direction is coincident with the incident direction) $\Phi_x = \Phi_i$, and σ_0 is that value corresponding to the backscatter angle Φ_i, as it should. For other cases, the scattering coefficient in the forward direction at an angle $\Delta\Phi_s$ from the specular direction is the same as the backscatter coefficient at half that angle from the normal. For example, from the equation above, the forward scattering coefficient at 90° from the specular direction would be the same as the backscattering coefficient at 45° from the vertical.

With a symmetrical backscatter relationship, the forward scatter relation can be obtained simply as the backscatter relation centred about the specular direction and with its angular axis doubled.

FIGURE 7

Geometric optics approximation of ground echo in the plane-of-reflection

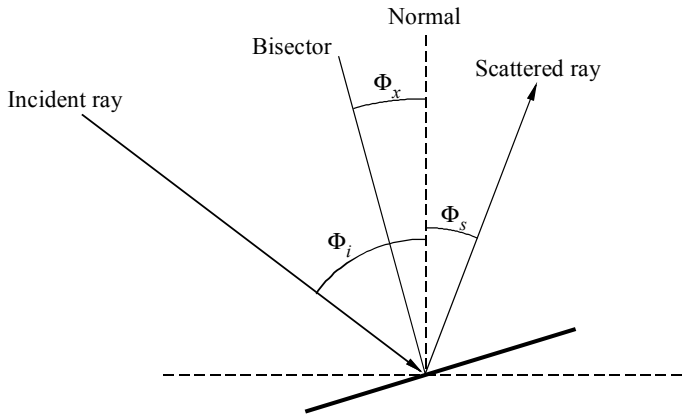

We can extend this process to the out-of-plane direction. Figure 8 illustrates the case where a portion of the incident power is scattered out-of-plane. $\vec{V}_i$ is a unit vector pointing in the direction from which the incoming radiation arrives. $\vec{V}_s$ is a unit vector pointing in the direction of the sensor bearing satellite. $\vec{V}_{bi}$ lies in the plane of $\vec{V}_i$ and $\vec{V}_s$ and bisects the included angle between the two. The facets determining the power reflected in the forward $\vec{V}_s$ direction would be

those normal to the vector $\vec{V}_{bi}$. As before, it would be the angular position of the bisector with respect to the normal that would set the value of σ_0. In vector notation (the summation, as described, always forms the bisector whenever $\vec{V}_i$ and $\vec{V}_s$ are unit vectors):

$$\vec{V}_{bi} = \left(\vec{V}_i + \vec{V}_s\right)$$

and (the magnitude of $\vec{V}_{nor}$ is included only for completeness as its value is unity by definition):

$$\Phi_x = \arccos\left(\vec{V}_{bi} \cdot \vec{V}_{nor} \Big/ \left|\vec{V}_{bi}\right|\left|\vec{V}_{nor}\right|\right)$$

FIGURE 8

Geometry for out-of-plane scattering

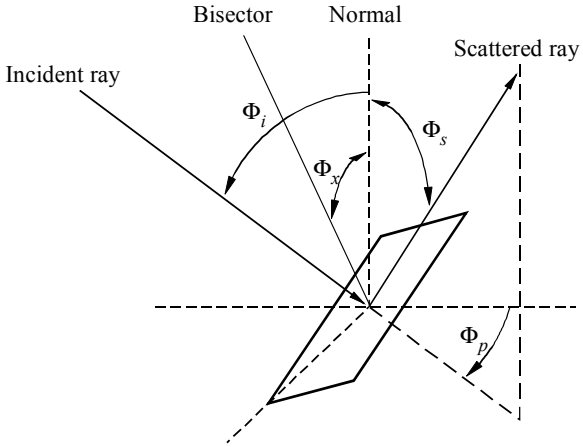

Evaluating the mean scattering coefficient corresponding to Φ_x for the out-of-plane case, one would get a contour plot as given in Fig. 9 when the incident angle, $\Phi_i = 45°$.

FIGURE 9

Contours of constant forward reflection coefficient

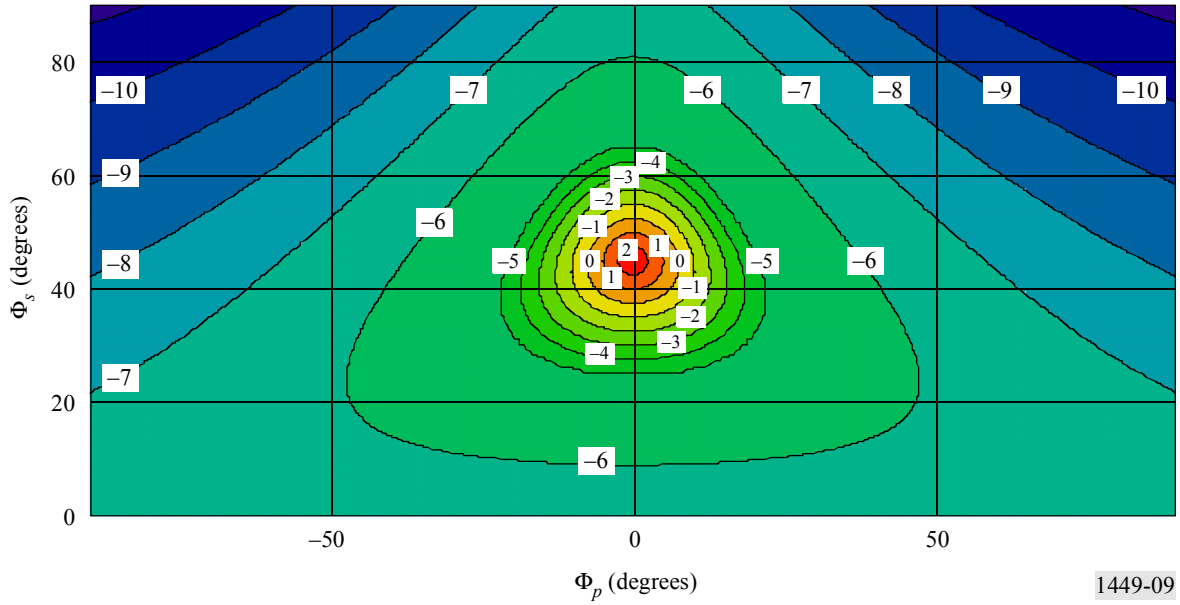

Note that the maximum energy is concentrated in the specular direction ($\Phi_p = 0$, $\Phi_s = 45$). Also note the pattern is nearly symmetric about the specular direction, in the vicinity of the specular direction, but significantly departs from symmetry for areas remote from that direction.

4 Results

4.1 Conditional interference statistics

We first consider the question of what percentage of sensor measurements would be expected to be corrupted given that the sensor is within a fixed-satellite coverage area. In a multi-beam coverage area such as described in § 2, the FSS coverage can encompass an entire administration such as the continental United States of America. In such an instance, the pixel loss within that administration would be critical. The conditional statistics provide that information. To obtain these statistics, we limit the sensor over-flight to a rectangular area which just encloses a generic fixed-satellite coverage area as described in § 2. Repeated over-flights were simulated with random assignment of ascending node, and interference data accumulated only while within a rectangle with latitude span of 20° to 55° N, and a longitude span of –130° to –52° W. Each orbit sub-segment was from a northern pass, which ordinarily would be from the Equator to the North Pole. Limiting the data to such sensor transits is intended as an interference mitigation technique. The resulting interference probability density and exceedence distribution are shown in Fig. 10 for the instance where each of 16 FSS GSO satellites produce a pfd of –101 dB(W/(m^2 · 200 MHz)) in each of two polarizations for each of 22 adjacent spot beams. These satellites are arranged in groups of four with common channelization plans such that each spot would scatter energy overlapping the EESS band from only four of the total (see § 2).

FIGURE 10

Interference for groups-of-four case with pfd of –101 dB(W/(m^2 · 200 MHz)) in both polarizations of 22 adjacent spot beams

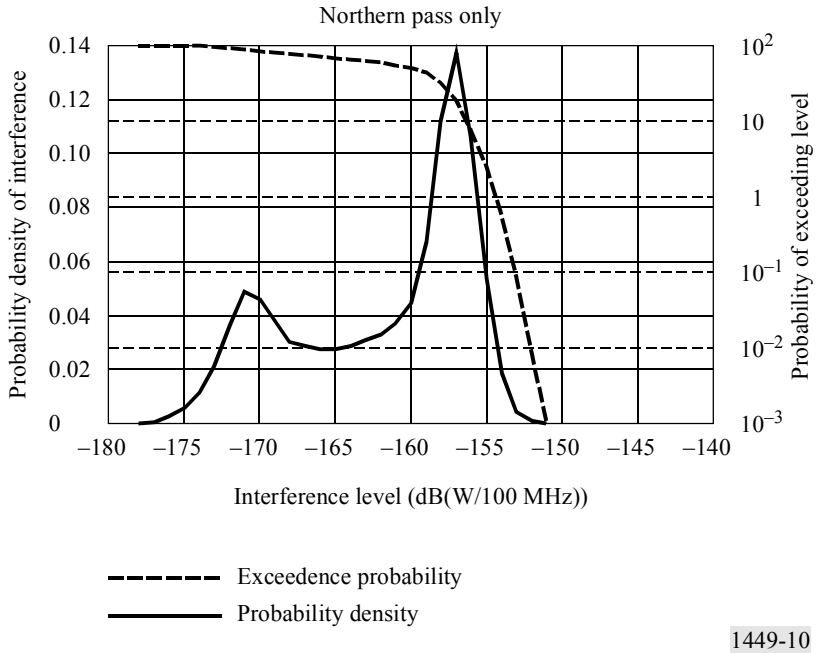

The probability density of the interference has two modes, one just under –170 dB(W/100 MHz) and the other near –157 dB(W/100 MHz). The upper mode corresponds to the peaks of the FSS spot beams while the lower level corresponds approximately to the sidelobe pedestal of the Recommendation ITU-R S.672 antenna pattern. For this scenario, the interference criterion (–155 dB(W/100 MHz)) would be exceeded for 2.4% of the pixels. This is about half the allowable amount for random occurrences (5%). The knee for the exceedence distribution is at about the 20% occurrence level.

4.2 Extrapolation to the unconditional (global) case and other FSS pfd values

Section 4.1 describes the pixel loss given that the sensor is over a GSO FSS coverage area. In instances where the sensor application service area is global, it is of interest to know the global pixel loss. Herein, we estimate global loss statistics by scaling the conditional case by the ratios of FSS area/total Earth land area. The total land area of the Earth is 147 million km^2. This is about 29% of the total surface area of the Earth (511 million km^2). Of this, FSS coverage would likely be limited to latitudes below 60° N (elevation restrictions) and 40° S (population distribution). By manually scanning a map of this region, the maximum FSS coverage is about 86% of the total. Consequently the maximum FSS coverage is about 25% (0.86×0.29) of the total Earth's surface. The scaling of exceedence occurrence rates to the global case is then:

$$P(I > X / Over\ Land) = P(I > X / FSS\ Coverage\ Area) \cdot P(FSS\ Coverage\ Area / Over\ Land)$$

From the above:

$$P(FSS\ Coverage\ Area / Over\ Land) = 0.86$$

Scaling for different GSO pfd limits is accomplished by shifting the exceedence curves to the right by the amount the new pfd exceeds –101 dB(W/(m^2 · 200 MHz)).

4.3 Occurrence rates of excessive pixel loss

The methods in prior sections were used to generate the results in Table 3. The results reported in Fig. 10 are dependent on the assumption of a maximum deployment of 16 FSS systems per coverage area, all providing overlapping, dual-polarization coverage to 24 spot beams. Additional scenarios of 4 and 8 satellites per FSS coverage area were also examined. If the allowable FSS pfd limit is fixed at –101 dB(W/(m^2 · 200 MHz)), the exceedence distributions for systems having 4, 8, and 16 systems per FSS coverage area is illustrated in Fig. 11. The 16 system case has four common interferers per spot beam, the 8 system case two, and the four system case one. For a particular exceedence probability, the interference level is reduced approximately by the ratio of number of interferers per spot.

FIGURE 11

Exceedence distributions

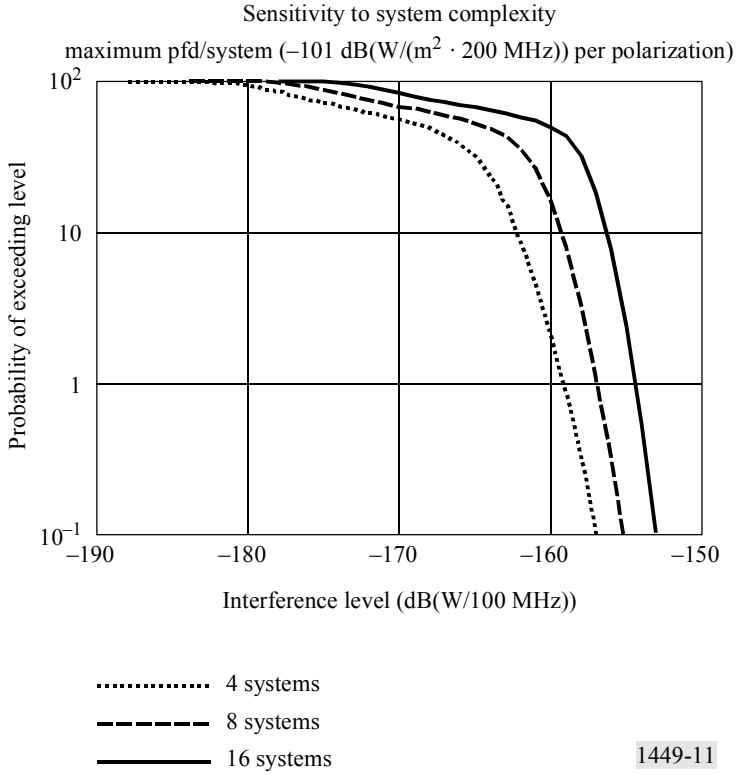

TABLE 3

Coverage loss for various FSS pfd values

pfd (dB(W/(m^2 · 200 MHz)))	Data loss over FSS service area (%)			Data loss over all land masses (%)		
	4	8	16	4	8	16
–101			2.4			2.1
–100		0.3	7.8		0.3	6.7
–99	0.1	1.1	18.4	0.1	1.0	15.8
–98	0.3	3.2	32.1	0.3	2.8	27.6
–97	0.8	7.9	43.3	0.7	6.8	37.2
–96	2.0	16.1	50.1	1.7	13.8	43.0
–95	4.4	26.5	54.5	3.7	22.8	46.9
–94	8.6	36.3	58.3	7.4	31.2	50.1
–93	14.9	43.6	61.6	12.8	37.5	52.9
–92	22.9	48.7	64.6	19.7	41.8	55.6
–91	31.5	52.6	67.5	27.0	45.2	58.0
–90	38.9	56.1	70.3	33.5	48.2	60.4
–89	44.7	59.2	73.0	38.4	50.9	62.8
–88	49.4	62.2	75.9	42.5	53.5	65.3
–87	53.3	65.2	78.9	45.8	56.1	67.9
–86	56.7	68.1	82.7	48.8	58.5	71.1
–85	59.9	71.0	87.3	51.5	61.0	75.1
–84	63.1	74.3	92.2	54.2	63.9	79.3
–83	66.2	78.1	95.8	56.9	67.2	82.4
–82	69.4	82.8	98.0	59.7	71.2	84.2

The 1% systematic interference criteria is exceeded for all pfd values in the 16 satellite case but is not exceeded for pfd limits less than –98 dB(W/(m^2 · 200 MHz)) in the 8 satellite case, nor is it exceeded for pfd limits less than –96 dB(W/(m^2 · 200 MHz)) in the 4 satellite case. The 5% random events criteria is met by several cases.

4.4 Sensitivity to sensor scan range

It has been proposed that under certain circumstances a degree of interference mitigation can be achieved by reducing sensor scan range. The approach was tested with the scenario described in § 2 and found to realize insignificant benefit.

The solid lines in Fig. 12 reiterate previous analyses that included a ±70° scan of the sensor. The symbols represent the same case with scan reduced to ±35°. Further testing of the concept revealed there was some advantage where the scattering coefficient was dominantly specular. Otherwise, the benefit was, indeed, insignificant.

FIGURE 12

Effect of restricted scan range of sensor

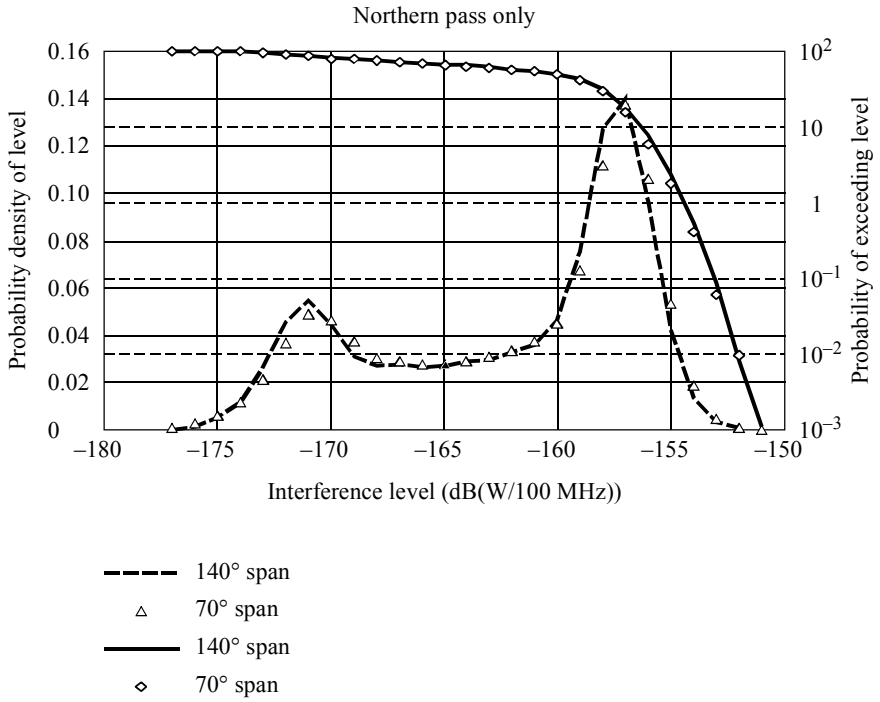

5 Conclusions

This Annex examined the data loss experienced by the passive sensor for a variety of FSS pfd limits ranging from −101 dB(W/(m^2 · 200 MHz)) to −82 dB(W/(m^2 · 200 MHz)). The study determined the passive sensor data loss for a variety of FSS deployment scenarios ranging from 4 FSS satellites to 16 FSS satellites per FSS coverage area. The results are given in Table 3.

These values were derived with the assumption that the entire world's land masses were all serviced by the same distribution of FSS systems. This is clearly not the case as many areas of the world would require four or less FSS satellites to service a given area while very few areas of the world would require as many as 8 to 16 FSS satellites to meet their communications needs. When this uneven distribution is taken into account on a worldwide basis and the sensor is further limited to taking data in only 50% of its orbit (i.e., while travelling towards the poles), the pfd limit which allows passive sensor operations to acquire a satisfactory amount of useful data over land masses on a worldwide basis is −95 dB(W/(m^2 · 200 MHz)). It should be noted that passive sensors that acquire data exclusively over ocean regions will experience far less data loss than the values shown in Table 3 and could therefore acquire data over their entire orbits over oceans. Therefore, this pfd limit would protect ocean sensing applications to a higher degree.

ANNEX 2

Sharing between spaceborne passive sensors and HEO satellites in the FSS in the 18.6-18.8 GHz band

1 Introduction

The purpose of this Annex is to investigate sharing between FSS systems in HEO and passive sensors. In addition, the 50% duty cycle passive sensor mitigation technique, described in Annex 1, is tested against the FSS systems.

Due to the antenna discrimination of the passive sensor (a front to back ratio of 74 dB is assumed in this Annex), previous studies have found that the reflected interference power dominates direct path interference power. That is, FSS downlink power that is reflected from the Earth into the sensor main beam exceeds the interference power that travels directly from the FSS satellite into the sensor antenna back lobe. Therefore, this study treats only the reflected component of interference power.

2 Spaceborne passive sensor parameters

The parameters assumed for the passive sensor are based on Recommendations ITU-R RS.515, ITU-R RS.1028, and ITU-R RS.1029 and are the same as those given in Annex 1. The availability criteria for the passive sensor is based on Recommendation ITU-R RS.1029 which states that in shared frequency bands (except in the absorption bands) the interference levels given above (−155 dB(W/100 MHz) for 18.6-18.8 GHz) can be exceeded for less than 5% of all measurement cells within a sensor's service area in the case where the loss occurs randomly, and for less than 1% of measurement cells in the case where the loss occurs systematically at the same locations.

In this study, losses are assumed to be systematic.

The interference results presented in the following sections assume that the sensor service area is global. This corresponds to a sensor which operates continuously and measures some parameter, for example water vapour, over both land and sea. The assumption of a restricted sensor service area will produce interference results which are better or worse that those for the global service area assumption depending on the distribution of FSS earth stations.

3 FSS parameters

The FSS parameters assumed for the HEO systems in this study are based primarily on USCSID. USCSID is a United States of America space system composed of 12 GSO and 8 HEO satellites that operate in the FSS. The HEO component of USCSID is referred to as USCSID-P. The 8 HEO satellites are in eight orbital planes with an orbital period of 11 h 58 min.

USCSID includes multiple ground terminals of two types. The first type of ground terminal has a large antenna (20 m) and is used for transmitting and receiving. The second type of ground terminal is transportable and has a smaller antenna that is used only for receiving. USCSID communication downlinks operate in the 18.0 to 21.2 GHz band. Uplinks and downlinks use both left-hand and right-hand circular polarization. The satellites use on-board signal processing. Coordination information on USCSID has been filed with ITU.

For this study, the minimum elevation angle for the HEO systems was chosen to be 10°. Orbital parameters of the FSS systems are given in Table 4.

TABLE 4

FSS orbital parameters

	HEO-8	HEO-12	HEO-24
Apogee (altitude) (km)	26 784	39 400	47 103
Perigee (altitude) (km)	1 000	1 000	24 469
Period (s)	28 721.33	43 082	86 164
Eccentricity	0.636	0.72	0.268
Inclination (degrees)	63.4	63.4	63.4
Argument of perigee (degrees)	270	270	270

Link parameters for the FSS systems are shown in Table 5.

TABLE 5

HEO FSS link parameters

Altitude (km)	7 500	12 000	20 000
Power (dBW)	9.5	12.5	15
Power in 100 MHz (dBW)	–6.6	–3.6	–1.1
Antenna gain (dBi)	51.0	51.0	51.0
pfd at nadir (dB(W/(m^2 · 100 MHz))	–104.1	–105.2	–107.1
pfd at nadir dB(W/(m^2 · 200 MHz))	–101.1	–102.2	–104.1

The HEO systems use power control because of varying altitude. Below 7 500 km the power is turned off. Between 7 500 and 12 000 km the power is 9.5 dBW, etc.

4 Scattering coefficient

In this study, the forward scattering coefficient is assumed to be a function of a single variable, the off-specular angle. The off-specular angle is the angle between:

– the direction in which the energy is scattered to the measurement receiver;

– the direction of specular reflection.

Because of this assumption, the scattering coefficient is circularly symmetric around the direction of specular reflection.

The forward scattering coefficient used is shown in Fig. 13. Note that a scattering coefficient of 0 dB corresponds to a situation in which the scattering surface acts as an isotropic scatterer, i.e. a surface that scatters energy equally in all directions. Thus, there is no paradox with a coefficient greater than 0 dB.

FIGURE 13

Scattering coefficient

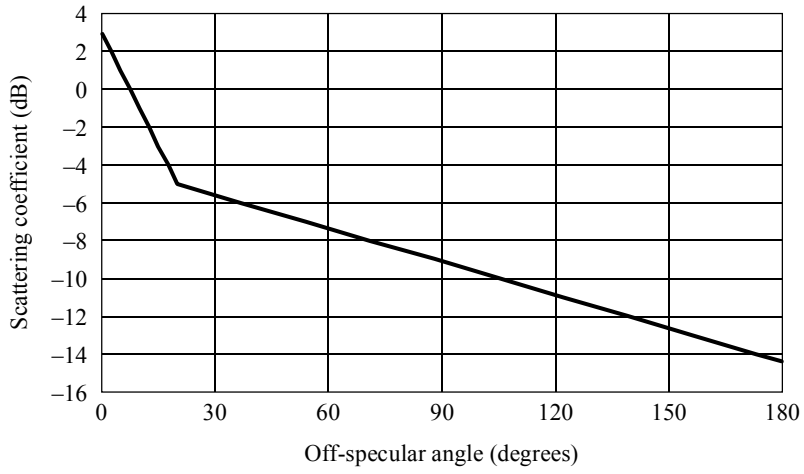

5 Interference power received by spaceborne passive sensor

Due to the antenna discrimination of the passive sensor (a front to back ratio of 74 dB is assumed in this Annex), the reflected interference power dominates direct path interference power. That is, FSS downlink power that is reflected from the earth into the sensor mainbeam exceeds the interference power that travels directly from the FSS satellite into the sensor antenna back lobe. Therefore, this study treats only the reflected component of interference power.

The reflected interference power received by the passive sensor, P_R, is given by equation (1).

$$P_R = dfp \frac{1}{\cos(\theta_R)} \frac{\lambda^2 \pi}{64} \sigma_0 L_T L_R L_P \quad (1)$$

where:

pfd: power flux-density of FSS transmitter measured at the Earth's surface

θ_R: passive sensor angle of incidence, measured from vertical

σ_0: scattering coefficient

L_T: atmospheric losses along path from FSS transmitter to scattering area

L_R: atmospheric losses along path from scattering area to sensor

L_P: polarization loss.

6 Interference simulation

The statistics of HEO FSS satellites interfering with a passive sensor were determined using computer simulation. For each simulation, a single FSS satellite was used. The reason for this approach was to illustrate the effects of the HEO geometry rather than model a particular multiple satellite system. Paragraph 7 discusses how the results can be scaled to represent multiple satellite systems.

In order to fix the relative positions of orbits, no perturbation was used. Each simulation was run for 200 days with a time increment of 10 s. The time increment equals the minimum time required for the passive sensor to cross the FSS 3 dB footprint.

A polarization loss of 1.5 dB was assumed corresponding to the isolation between linear and circular polarization. The atmospheric attenuation model from Recommendation ITU-R P.618 was used. The atmospheric conditions assumed were clear air, water vapour pressure of 7.5 g/m^3, and a temperature of 15° C.

One passive sensor interference mitigation technique is that the sensor is turned on when travelling away from the Equator and turned off when travelling toward the Equator. This technique is effective against FSS GEO systems since the off-specular angle is usually large when the sensor is travelling away from the Equator.

The simulation was run for the away from Equator case just described. It was also run for a continuously operating sensor, and, for completeness, for a toward Equator case. In the toward Equator case, the sensor is turned on when approaching the Equator and turned off when travelling away from the Equator.

7 Simulation results

The simulations assume a single HEO FSS satellite and a single FSS earth station. HEO satellite systems are usually used for communication with earth stations at mid to high latitudes. For this reason the earth station latitude was set to 40° N. The earth station longitude was set equal to the longitude of the HEO apogee.

7.1 Eight-hour HEO interferer

The cumulative interference distributions for an 8 h period HEO interferer are shown in Figs. 14, 15, and 16. The time percentage is normalized to the amount of time the sensor is turned on. The plots show the per cent of time the interference level exceeds the abscissa value.

FIGURE 14

Per cent of time interference exceeds abscissa value, 8 h HEO interferer, geometry 1

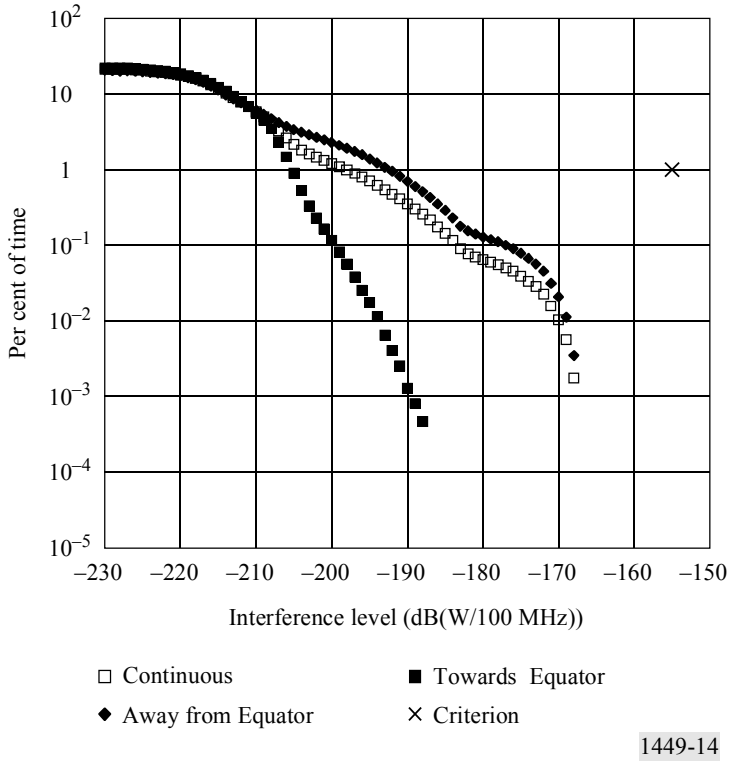

FIGURE 15

Per cent of time interference exceeds abscissa value, 8 h HEO interferer, geometry 2

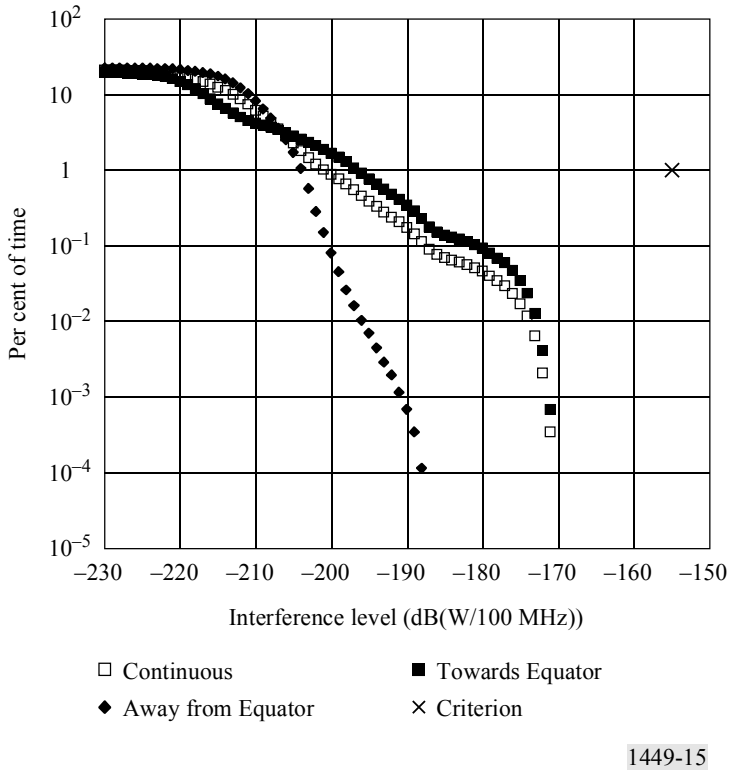

FIGURE 16

Per cent of time interference exceeds abscissa value, 8 h HEO interferer, geometry 3

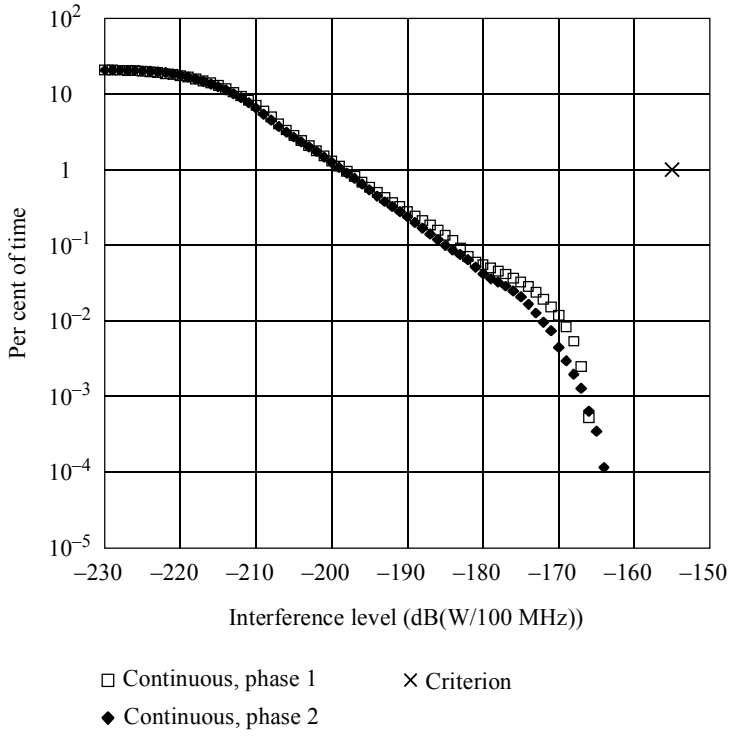

1449-16

In geometry 1 (Fig. 14) and geometry 2 (Fig. 15) the passive sensor orbital plane passes through the apogee of the interferer orbit. In geometry 1, the passive sensor is moving away from the Equator as it passes beneath the HEO apogee. In geometry 2, it is moving toward the Equator. Geometries 1 and 2 are illustrated in Fig. 17.

FIGURE 17

HEO interferer, geometries 1 and 2

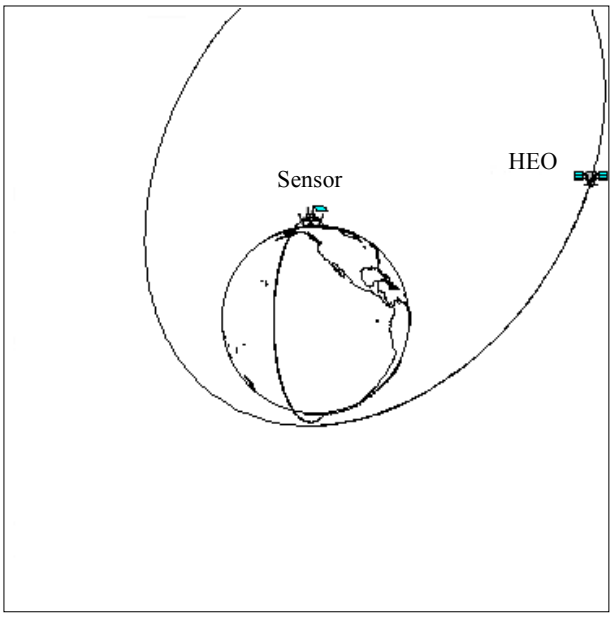

1449-17

In geometry 3 (Fig. 16) the passive sensor orbital plane is 90° away from its orientation in geometries 1 and 2. There are two phases in geometry 3. In phase 1, the passive sensor ascending node is west of the HEO apex. In phase 2, the passive sensor ascending node is east of the HEO apex. Geometry 3 is illustrated in Fig. 18.

FIGURE 18

HEO interferer, geometry 3

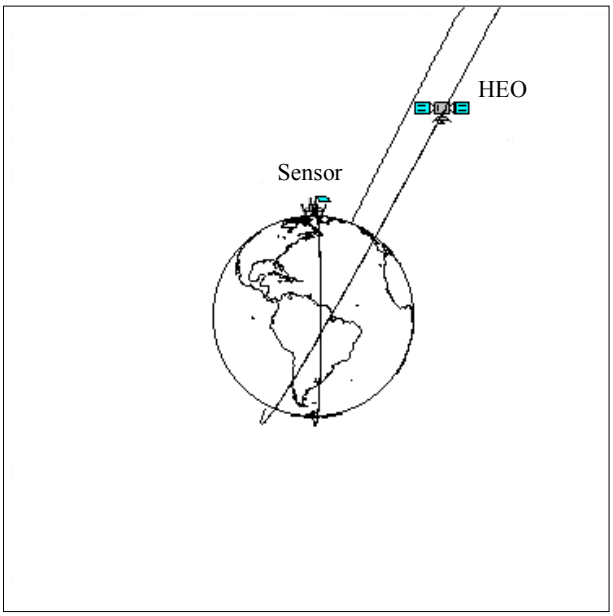

In Fig. 14, the towards Equator case, the sensor does not see the FSS earth station when it is being illuminated and thus receives much less interference. This also happens in Fig. 15 in the away from Equator case.

7.2 Twelve-hour HEO interferer

The cumulative interference distributions for a 12 h period HEO interferer are shown in Figs. 19, 20, and 21. The 12 h HEO orbit is frequently referred to as a Molniya orbit.

Note that in Fig. 20 the discontinuities in the three curves at the interference level = −187 dB(W/100 MHz) are caused by the side lobe structure of the FSS satellite antenna pattern (Recommendation ITU-R S.672).

7.3 Twenty-four-hour HEO interferer

The cumulative interference distributions for a 24 h period HEO interferer are shown in Figs. 22, 23 and 24. The 24 h period HEO orbit is frequently referred to as a Tundra orbit.

The level of interference with HEO systems obviously depends strongly on the relative orbital geometry. Using the worst cases from the Figs. 22, 23 and 24 provides a bound on interference levels for any geometry.

FIGURE 19

Percent of time interference exceeds abscissa value, 12 h HEO interferer, geometry 1

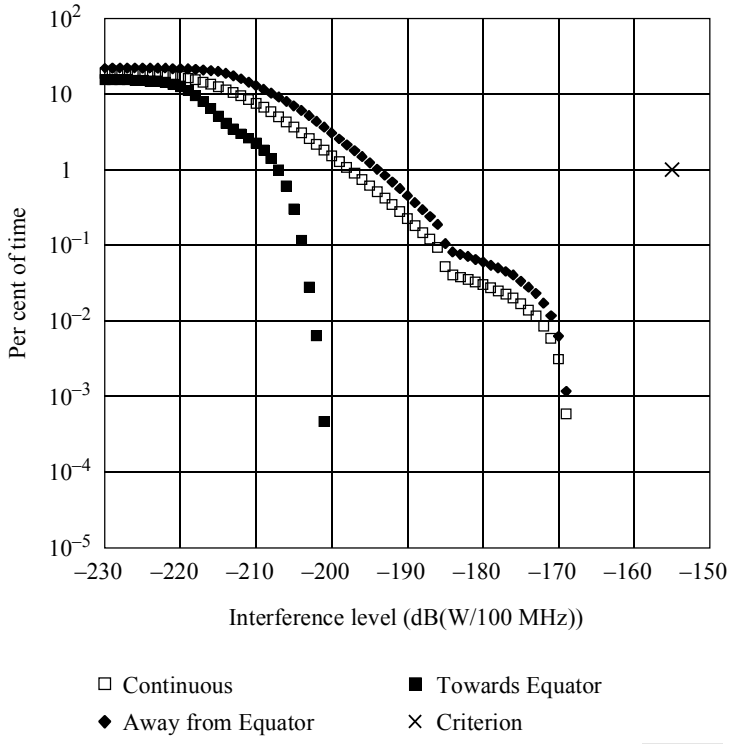

1449-19

FIGURE 20

Per cent of time interference exceeds abscissa value, 12 h HEO interferer, geometry 2

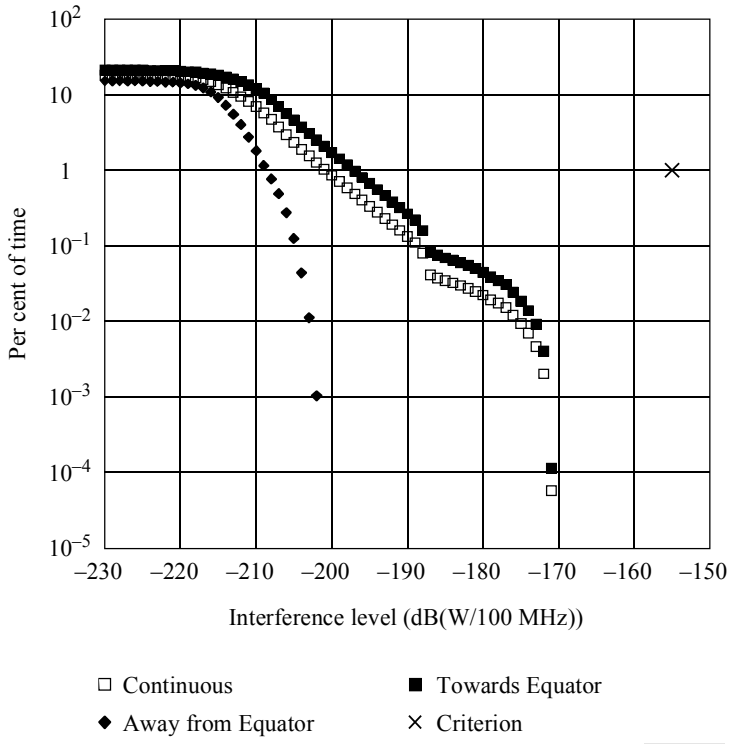

1449-20

FIGURE 21

Per cent of time interference exceeds abscissa value, 12 h HEO interferer, geometry 3

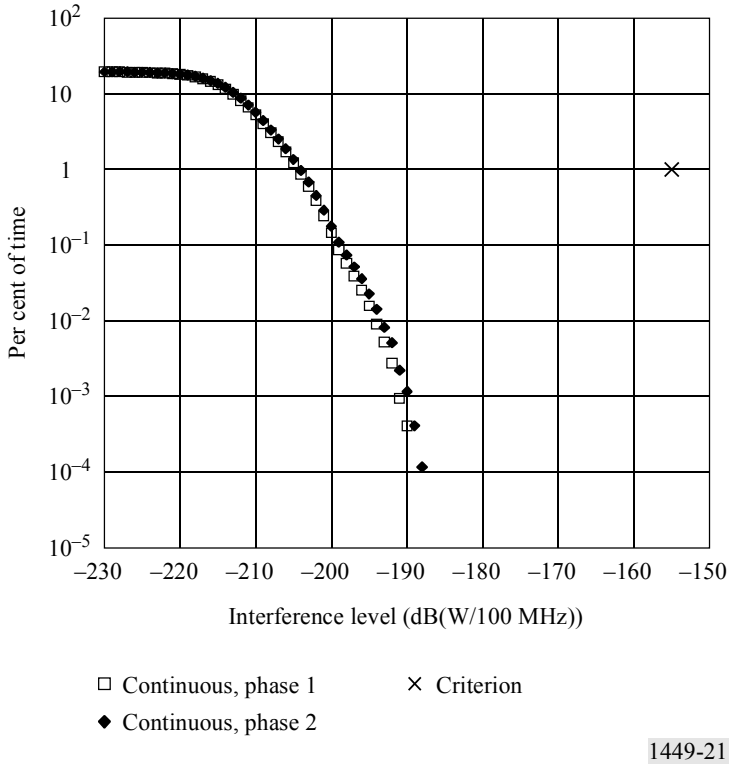

FIGURE 22

Per cent of time interference exceeds abscissa value, 24 h HEO interferer, geometry 1

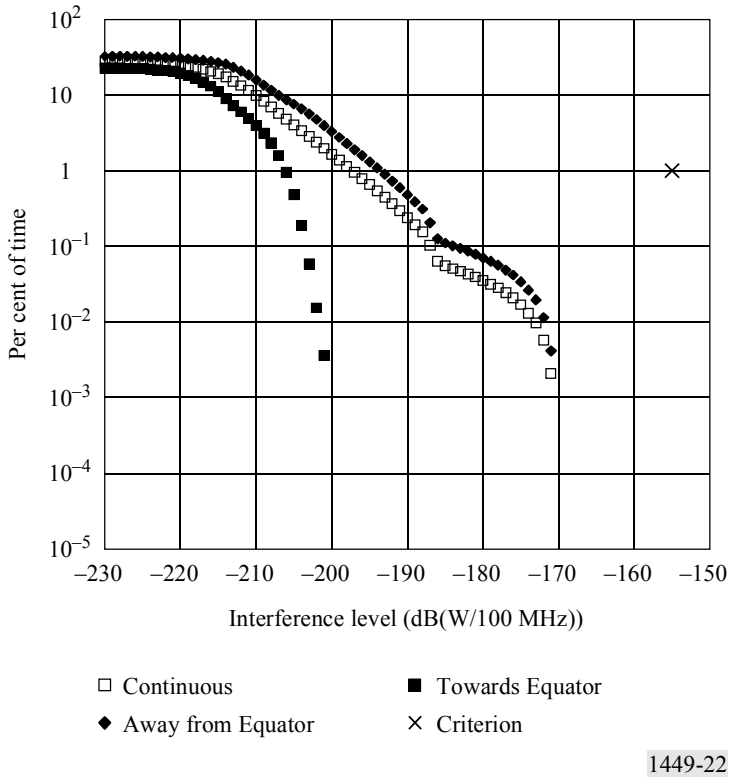

FIGURE 23

Per cent of time interference exceeds abscissa value, 24 h HEO interferer, geometry 2

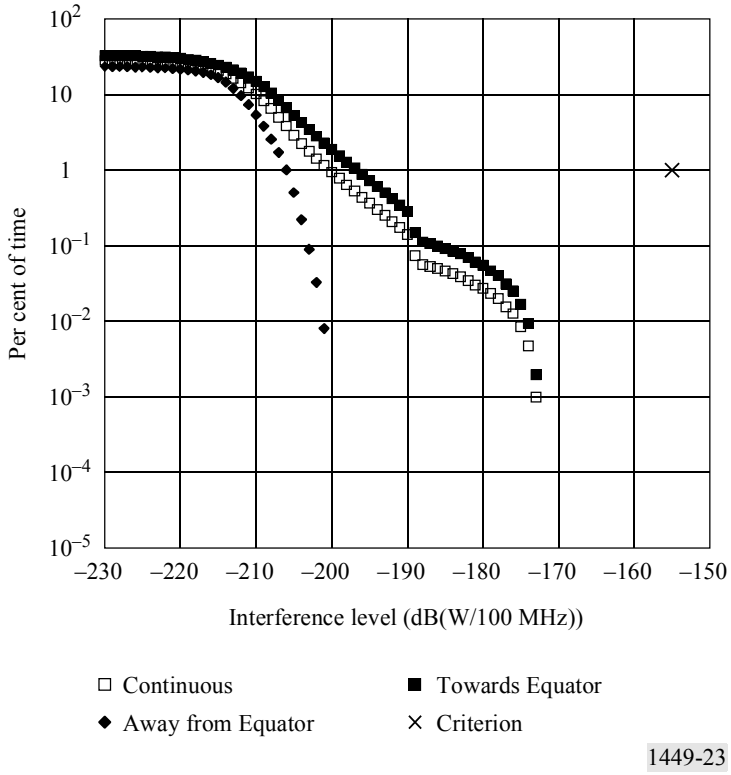

FIGURE 24

Per cent of time interference exceeds abscissa value, 24 h HEO interferer, geometry 3

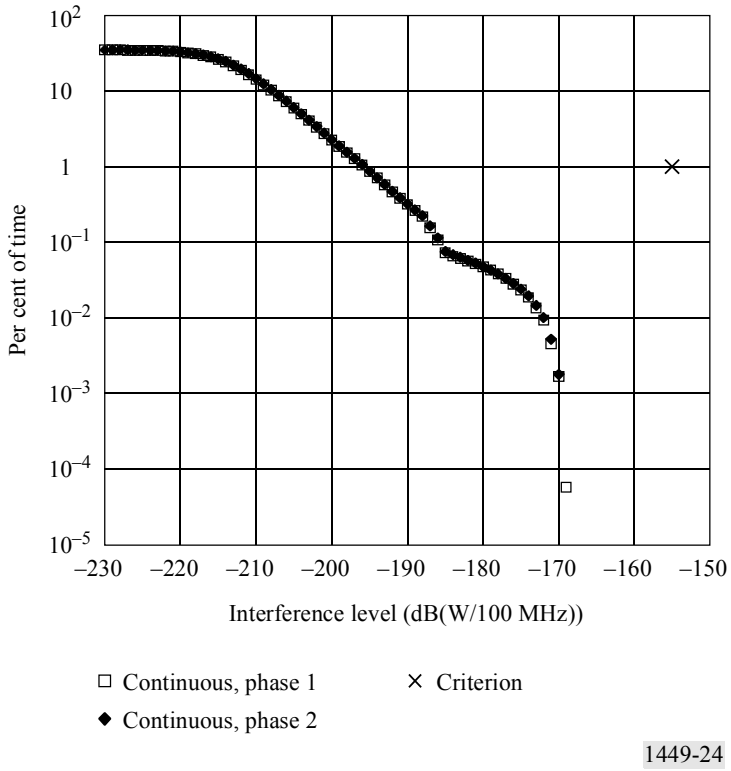

7.4 Scaling of results

All results presented in this Annex are based on a single FSS satellite interfering with a passive sensor. These results can be scaled up to multiple identical interfering satellite situations in two limiting cases. First, if the scattering region is to be exposed to *N* interfering satellites simultaneously, then each interference event may be increased in power by as much as 10 log (*N*) dB. The power increase is generally less than 10 log (*N*) dB since neither the interfering satellites nor the associated earth stations are collocated. This can be visualized on the interference charts by moving the curves to the right by 10 log (*N*) dB.

Second, if there are *N* interfering satellites, but the passive sensor is exposed to only one interfering signal at a time, then the time percentage corresponding to each interference level may be multiplied by the factor of *N*. This can be visualized on the interference charts by moving the curves up (vertically) by a factor of *N*.

Finally, of course, for a single interfering satellite with a power level different from that assumed in the simulations, the interference curves may be adjusted to the right or left by the appropriate amount. Specifically, for a maximum pfd of –95 (dB($W/m^2 \cdot 200$ MHz)), the interference curves can be moved to the right by 5.9 dB. This is based on the link parameters shown in Table 5. These scaling techniques can be used to approximately evaluate numerous satellite scenarios.

8 Conclusions

For none of the single satellite, single beam cases simulated is the passive sensor interference criterion exceeded. However, application of these results to complex systems requires scaling the results as discussed in the previous section. This involves shifting the curves to the right and upward by amounts that depend on system complexity.

Determining exact interference statistics for multi-satellite, multi-beam systems requires simulation that is more complex. Nevertheless, it can, in general, be concluded that a complex multi-satellite HEO system would still provide significant power margin and that the proposed mitigation technique causes little change in the interference received from HEO FSS systems with earth stations at mid-latitudes.